

Low-Cost Anti-Copying 2D Barcode by Exploiting Channel Noise Characteristics

Ning Xie, *Senior Member, IEEE*, Qiqi Zhang, Ji Hu, Gang Luo, and Changsheng Chen, *Member, IEEE*

Abstract—In this paper, for overcoming the drawbacks of the prior approaches, such as low generality, high cost, and high overhead, we propose a Low-Cost Anti-Copying (LCAC) 2D barcode by exploiting the difference between the noise characteristics of legal and illegal channels. An embedding strategy is proposed, and for a variant of it, we also make the corresponding analysis. For accurately evaluating the performance of our approach, a theoretical model of the noise in an illegal channel is established by using a generalized Gaussian distribution. By comparing with the experimental results based on various printers, scanners, and a mobile phone, it can be found that the sample histogram and curve fitting of the theoretical model match well, so it can be concluded that the theoretical model works well. For evaluating the security of the proposed LCAC code, besides the direct-copying (DC) attack, the improved version, which is the synthesized-copying (SC) attack, is also considered in this paper. Based on the theoretical model, we build a prediction function to optimize the parameters of our approach. The parameters optimization incorporates the covertness requirement, the robustness requirement and a tradeoff between the production cost and the cost of illegally-copying attacks together. The experimental results show that the proposed LCAC code with two printers and two scanners can detect the DC attack effectively and resist the SC attack up to the access of 14 legal copies.

Index Terms—Two-dimensional barcodes, anti-copying, illegal channel, theoretical modeling.

I. INTRODUCTION

Two-Dimensional (2D) barcodes are widely used in various applications because of their advantages of simple and low cost. In addition, one attractive feature in 2D barcodes is capable of providing significantly higher information capacity than that in 1D barcodes [1], [2]. A 2D barcode pattern named Quick Response (QR) code has been popularly used in our daily life. For example, a QR code can be employed as the information entrance of an advertisement, the information carrier for a mobile payment transaction, and a product authentication for tracking and anti-counterfeiting, etc.

Recently, the security of 2D barcodes has received extensive attention due to the following three major security risks [3]–[8]. First, various types of illegal information, e.g., Trojan virus and phishing websites, are encoded in a normal 2D barcode. It is challenging to detect illegal information before the barcode is decoded [9]. Second, a 2D barcode can be illegally tampered by a replacement attack that covers the original barcode by an illegal one. Under such attacks, some important information, e.g., the payee of a mobile payment transaction, can be tampered and it results in may cause some economic loss [10]. Third, a 2D barcode can be illegally replicated to fake a unique identifier in a tracking system for the anti-counterfeiting application.

The first two security risks have been effectively overcome. For example, for the first security risk, an anti-virus and anti-phishing recognition mechanism was used before the receiver of a 2D barcode executes the decoded information [11], while for the second security risk, the digital signature algorithms can be used to check the authenticity and integrity of the contents in a 2D barcode [12]. However, the third security risk (illegal copying) is more challenging as compared with the other two risks, since a 2D barcode can be easily replicated with an off-the-shelf photocopier. An illegal copying 2D barcode not only leads to large economic and reputational loss for the authorized manufacturer but also limits the application of 2D barcodes as an anti-counterfeiting technique. Thus, this paper focuses on the problem of illegal copying.

In the literature, some approaches have been proposed to overcome the security risk of illegal copying but accompanying with some limitations. Now, we briefly introduce them as follow.

1) *Special Printing Materials or Techniques*. This approach exploits the special features of printing materials or techniques, which cannot be reproduced on purpose, to counter the attack of illegal copying. For example, a polymerized liquid crystal material [13] with unique optical characteristics can be used to print an anti-copying 2D barcode. Some red, green and blue light-emitting nano-particles [14] can be used to construct 3-dimensional (3D) QR codes that cannot be copied by ordinary technologies. Special halftone printing technology [15] can generate 2D barcodes that are invisible under visible light. However, this approach not only increases the production cost but also reduces the universal applicability of a 2D barcode, which hinders its promotion in extensive applications.

2) *Physical Unclonable Function (PUF)*. The PUF is an unclonable response function which inputs a stimulus to a physical entity and then outputs a unique feature according to the internal physical structure, e.g., a unique texture of printing paper [16]. In recent years, researchers have found that it is possible for a mobile imaging device under a semi-controlled condition to acquire images of paper and to extract microscopic textural features for constructing the PUF [17]. The PUF, which acts as a digital signature of each printing substrate, is stored in an online database to facilitate the verification of textural features extracted from a query document. This approach has a limitation. The authentication is performed over an online database, where the scale of the database has been greatly restricted. The scale of the database applied is often not sufficiently large to have extensive universality. When the scale of the database is expanded, the accuracy of its authentication will be reduced.

3) *Anti-copying Pattern*. Some patterns with detailed features, such as high-density black or white blocks, can be used to prevent illegal copying [18]. Similarly, the following

The authors are with the Guangdong Key Laboratory of Intelligent Information Processing, College of Information Engineering, Shenzhen University, Shenzhen, 518060, China (e-mail: ningxie@szu.edu.cn; cschen@szu.edu.cn).

patterns also can be used for anti-copying, e.g., the black-and-white texture pattern with a grating structure [19] and color anti-copying pattern which contains the information of four channels of CMYK [20]. This approach requires that the legal receiver equips a capturing device with a high resolution, which apparently increases the implementation cost of the receiver and is impractical for a low-cost mobile phone.

4) *Digital Watermarking*. The digital watermarking technology (DWT) can embed certain privacy information in a 2D barcode so as to protect its content authenticity [15]. Semi-fragile watermark is an important branch of DWT [21], which can resist distortion or tamper with low intensity and can detect distortion or falsification of various types of images with high intensity [22]. However, to our best knowledge, there is no public report that a digital watermarking technique has been used against illegally-copying attacks.

In summary, the existing anti-copying approaches have the drawbacks of low generality for special material, high cost for high-resolution equipment and high overhead for online database required. In this paper, we focus on the print-capture channel where a message is transmitted using a printed medium and is retrieved by a mobile imaging device. We propose a low-cost anti-copying (LCAC) 2D barcode by exploiting the difference between the noise characteristics of legal and illegal channels. At the same time, we propose some possible transformations of the 2D barcode, and give corresponding covertness and robustness analysis. For accurately evaluating the performance of the proposed LCAC code, a theoretical model of the noise in an illegal channel is established by using a generalized Gaussian distribution. At last, based on the theoretical model, we built a prediction function to optimize the parameters of the proposed LCAC 2D barcode in order to increase the cost of copying attack and achieve a better anti-copying effect.

The key contributions of this work can be summarized as follows.

- 1) We propose a low-cost anti-copying (LCAC) 2D barcode on the basis of the considered 2D barcode, which exploits the difference between the legal and illegal channels. In the proposed LCAC code, the sender of a 2D barcode embeds an authentication message into a source message to realize the anti-copying purpose. Two embedding strategies are proposed and analyzed.
- 2) For accurately evaluating the performance of the proposed LCAC code, a theoretical model of an illegal channel based on various printers and scanners is established by using a generalized Gaussian distribution. By comparing with the actual experimental results, the theoretical model works well.
- 3) For improving the security of the proposed LCAC code, besides the direct-copying attack, an improved version which is the synthesized-copying attack, is also considered in this paper. Based on the aforementioned theoretical model, we built a prediction function to optimize the parameters of the proposed LCAC code. The parameters optimization incorporates the covertness requirement, the robustness requirement and a tradeoff between the production cost and the cost of illegally-

copying attacks together. The experimental results show that our approach has a good ability to prevent illegal copying.

II. BACKGROUND OF CONSIDERED 2D BARCODE AND SYSTEM MODEL

A. Background of Considered 2D Barcode

Without loss of generality, this paper considers M -order multilevel 2D barcodes [12], where M is the modulation order and $M \geq 2$. The block diagram of the generic 2D barcode is illustrated in Fig. 1, as shown at the top of the next page. As shown in the sender of Fig. 1, $s_{c,1}$ denotes a source message with length $L_c = Nk$, where N is the number of blocks and k is the length per block. The $s_{c,1}$ is encoded via Reed-Solomon (RS) codes to obtain the coder output $s_{c,2}$. The output length of RS codes per block is denoted as n and its error correction capability is $t = (n - k) / 2$. Thus, the length of $s_{c,2}$ is $L_s = Nn$.

Then, through a pulse amplitude modulation (PAM) with order M [23], we obtain a modulated signal s_m . The modulate block transforms a bit stream into the corresponding gray-scale values. The case of $M = 2$ is very popular in the practical application of 2D barcodes; however, the cases of $M \geq 4$ is becoming a new research trend due to its high capacity [12]. Thus, this paper focuses on the case of $M = 4$. Following [24], the constellation points x are set as $x \in \{40, 100, 160, 220\}$, that is, $x_1 = 40$, $x_2 = 100$, $x_3 = 160$, $x_4 = 220$. Note that the ideas of this paper can be straightforwardly extended to other cases, e.g., $M = 2$ and $M = 8$.

After inserting the header and training symbols into the modulated signal s_m , the original version of a 2D barcode, s_d , is generated. The total length of header and training symbols is denoted as L_h and the final length of a 2D barcode is denoted as $L_t = L_s + L_h$, where the value of L_t should be an integer after taking a square root to keep the 2D barcode a square structure. The header symbols have two functions: first, it stores additional information, e.g., format and version of a considered 2D barcode; second, its length is adjustable to ensure that the value of L_t satisfies the length requirement in a considered 2D barcode [24].

In Fig. 2, the white and grey modules represent the modulated symbols of information bits and redundant bits of the source message, respectively. The yellow and red modules represent the locations of header symbols and training symbols, respectively. The intensity of red illustrates the gray level of the training symbols. Moreover, two types of training symbols are considered. The first type is used to estimate the spatial distortion, which is set over an entire 2D barcode as uniform as possible; the second type is used to estimate the post-processing distortion, which is set at the center area of a 2D barcode [24]. Following [24], the gray value of the first type of training symbols is set to 130, while those of the second type of training symbols are set to $\{30, 50, 70, 100, 160, 180, 200, 220\}$, as shown the red cross of Fig. 2. Note that, as the last step of encoding a 2D barcode, a finder pattern should be attached to facilitate the detection of a 2D barcode reader [25]; however, without

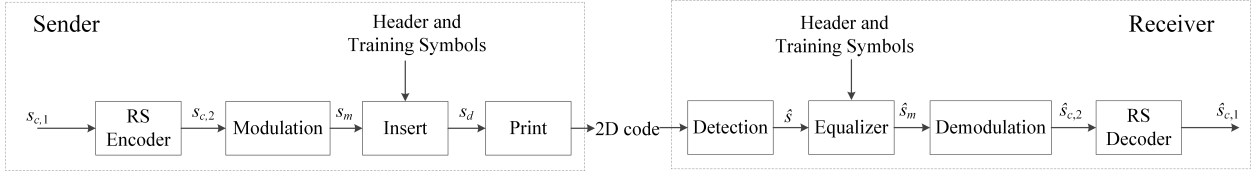


Fig. 1. Block diagram of the considered 2D barcode.

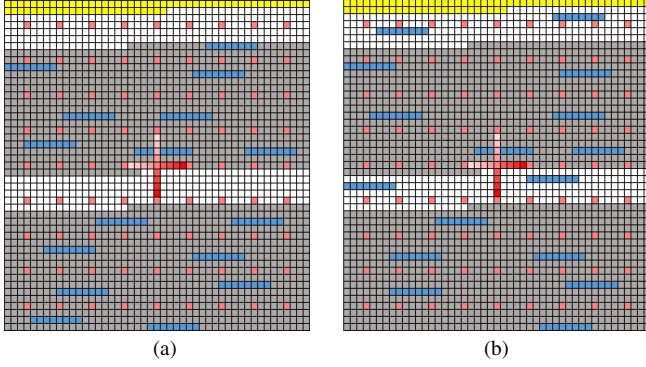


Fig. 2. Structure diagrams of LCAC codes, where the number of RS code blocks is 2 ($N = 2$), yellow and red modules represent the header and training symbols, respectively. The two diagrams are based on two different embedding strategies: (a) Strategy 1; (b) Strategy 2. In Strategy 1, the authentication message is randomly embedded into the redundant bits of the source message, whereas, in Strategy 2, the authentication message is randomly embedded into the entire bits of the source message.

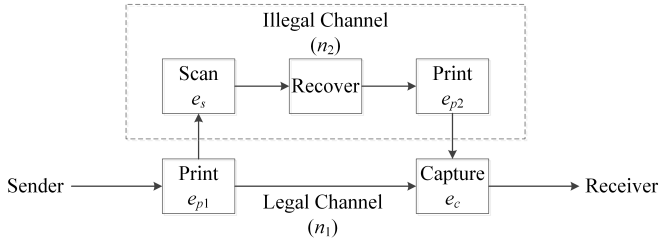


Fig. 3. The system model of a 2D barcode with two possible channels, *i.e.*, legal channel and illegal channel.

causing any confusion, the finder pattern is omitted in Fig. 1 for conciseness.

In Fig. 1, the first block of a receiver is the detection block which scans the printed 2D barcode with a mobile phone camera or an optical scanner. The detection block is to locate and to segment the captured version of a 2D barcode by using the finder pattern. Then, the detection block quantizes the mean intensity within each partitioned area to obtain a gray-scale signal \hat{s}_d . The \hat{s}_d is fed into an equalizer block which compensates the channel distortion by using the training symbols described above [24]. Specifically, the equalizer block trains a fitting function to reflect the channel distortion by comparing the gray-scale values of the scanned training symbols with those of the considered ones. The fitting function can be described by a sigmoid function in practical situations [24]. When the fitting function is trained, an inverse fitting function is further established to correct the distortions in \hat{s}_d . Then, \hat{s}_m is extracted by removing the header and training symbols in \hat{s}_d . Next, \hat{s}_m is demodulated and decoded to obtain $\hat{s}_{c,2}$ and $\hat{s}_{c,1}$, respectively.

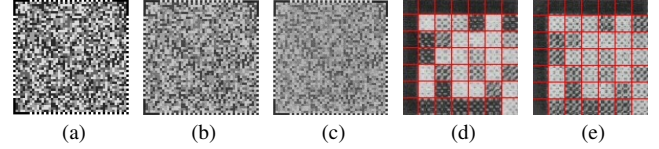


Fig. 4. Examples of a 2D barcode: (a) original 2D barcode; (b) captured legal 2D barcode; (c) captured illegally copied 2D barcode; (d) enlarged top-left region of a legal 2D barcode; (e) enlarged top-left region of an illegally copied 2D barcode.

B. System Model

As shown in Fig. 3, we consider the system model of a 2D barcode by two different channels, *i.e.*, a legal channel and an illegal channel. In the legal channel, as shown by the lower branch of Fig. 3, a legal 2D barcode is received through only a print-and-capture process, whereas in the illegal channel as enclosed by the dashed box of Fig. 3, an illegal 2D barcode is received through a print-scan-print-and-capture process, which is denoted as a double print & scan (DPS) process. Intuitively, the distortion and noise in an illegal channel are more serious than those in a legal channel. Specifically, the total noise in a legal channel can be modeled as

$$e_1 = e_{p1} \oplus e_c, \quad (1)$$

where e_{p1} and e_c represent the noise components of the first printing process and the legal detecting process, respectively, ' \oplus ' represents the interaction of noise in different stages. The more common relationships are additive noise and multiplicative noise. The total noise in an illegal channel is written as

$$e_2 = e_{p1} \oplus e_s \oplus e_{p2} \oplus e_c, \quad (2)$$

where e_s and e_{p2} denote the noise components of the illegal scanning process and the second printing process, respectively.

By considering the models of printing and scanning processes in [24], it is easy to conclude that $\sigma_{e_1}^2 < \sigma_{e_2}^2$ since more processes of printing or scanning introduce more noise. This conclusion is also demonstrated through an example shown in Fig. 4. By comparing the details of Fig. 4(a) with those of Fig. 4(b) and Fig. 4(c), the noise variance of the legal 2D barcode is slightly larger than that of the original barcode, whereas the noise variance of the illegally copied one is much larger than those of both the legal 2D barcode and the original barcode. Although it is possible to distinguish the illegally copied 2D barcode by detecting various characteristics of two channels [18], [26], it is challenging for a low-cost mobile terminal, *e.g.*, a mobile phone, to finish this task due to the following two reasons. First, it is difficult to set an appropriate threshold to distinguish two types of 2D barcodes, even for the enlarged subgraph as shown in Fig. 4(d) and Fig. 4(e), since there is no prior information for two types of channels. Second, if

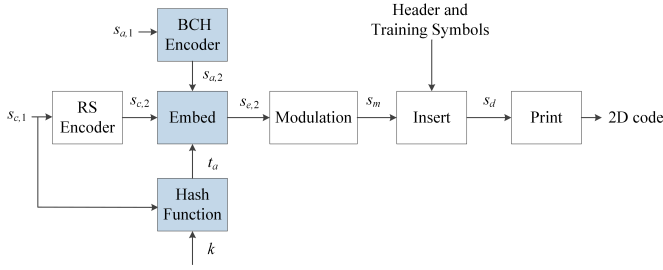


Fig. 5. Block diagram of the sender in the proposed LCAC code.

the mobile phone performs an authentication with the online database, which not only causes large network overhead but also introduces additional security risks due to the frequent sensitive data exposure during wireless communication. The basic idea of our approach is to embed an authentication message into a source message, where the decoded bit-error-rates (BER) of the authentication message is sensitive to the noise variance. In the receiver, we set an appropriate threshold for decoded BER of authentication message to detect whether the received 2D barcode is an illegally copied version of the legal 2D barcode or not, which will be described in the next section. Then, we fine-tune the performance of our approach by optimizing the embedding parameters of the authentication message, which will be described in Section VI.

III. THE PROPOSED LOW-COST ANTI-COPYING CODE

A. Description for the Sender

As shown in Fig. 5, we generate an authentication message $s_{a,1}$ for anti-copying purpose. The $s_{a,1}$ is encoded via the Bose-Chaudhuri-Hocquenghem (BCH) codes to obtain the coder output $s_{a,2}$ for improving its robustness. The lengths of $s_{a,1}$ and $s_{a,2}$ are denoted as k_a and n_a respectively, and the error correction capability is t_a .

The key block of the sender in the proposed LCAC code is the embed block which replaces certain bits of the source message by those of the authentication message. Specifically, if the bit of the source message is different from that of the authentication message, this bit is modified from 0 to 1 or 1 to 0; otherwise, this bit is kept unchanged. Apparently, the embedding operation sacrifices the robustness of the source message, which also can be denoted as the covertness of the authentication message. There are two aspects of the covertness requirement in our LCAC code. First, the presence of the authentication message should not be easily detectable by the illegal receiver. Second, it should not have a noticeable effect on the receivers' ability to recover the source message. Moreover, covert authentication in an LCAC code may be used together with other security techniques in the conventional approaches to produce a more secure 2D barcode. In this paper, the covertness performance is analyzed through the error probability of demodulation and decoding for the source message. The values of k_a and n_a , the parameters of the proposed LCAC code, should be optimized by jointly considering the covertness and robustness of authentication message, which will be analyzed in Section VI.

Besides the embedding length n_a , The embedding locations should be carefully designed as well. In this paper, we consider two embedding strategies to define different embedding locations. In the first strategy, as shown in Fig. 2(a), which is short as Strategy 1 for simplicity, $s_{a,2}$ is randomly embedded into the redundant bits of $s_{c,2}$. In the second strategy, as shown in Fig. 2(b), which is short as Strategy 2, $s_{a,2}$ is randomly embedded into the entire bits of $s_{c,2}$. In the sender of an LCAC code, the specific embedding locations are defined through a one-way, collision-resistant hash function with the source message and the secret key k , expressed as

$$t_a = g(s_{c,1}, k), \quad (3)$$

where the hash function $g(\cdot)$ is robust against input error for generating the random locations. The secret key k is generated and allocated by the sender. For higher security, k is different for different source messages $s_{c,1}$, which means that different keys are generated for different products. Before each verification attempt, the legal receiver sends an authentication request to the sender, and the sender feedbacks k and $s_{a,1}$ to the receiver via a secure way, e.g., encryption. Note that we can use some advanced key agreement protocols [27], [28] to achieve the allocation of secret keys for further improving the security of the considered 2D barcode.

Note that both k and $s_{a,1}$ are only secret information required in the LCAC codes and the exchange of secret information occurs only once, thus the overhead for anti-copying in the LCAC is very low. An alternative solution is to allocate both k and $s_{a,1}$ when the authentication program is installed into a mobile phone, which avoids the exchange of secret information. Note that, before a legal receiver accepts a 2D barcode, the authentication message should be treated as a noise signal as well since the legal receiver does not know whether the authentication message exists or not in the received signal.

For two embedding strategies, we have the following observations:

Observation 1: Strategy 1 has better covertness performance than Strategy 2 since the impact of errors occurred in the redundant bits to the decoding performance of source message is smaller than that in the information bits according to the coding structure of RS codes.

Observation 2: Strategy 2 has better robustness performance than Strategy 1 since Strategy 2 has larger embedding range, which spreads the authentication message into a larger area and lowers the error probability caused by some local distortion, e.g., a part of the 2D barcode is shaded.

Observation 3: Strategy 2 has better security performance than Strategy 1 since each bit of the authentication message is embedded in a larger space, which intuitively increases the uncertainty of detecting the authentication message by an adversary. The first two observations are verified through experimental results in APPENDIX A.

The two embedding strategies in LCAC codes are illustrated in Fig. 2 as two toy examples, where the case of $N = 2$ is considered. The blue modules represent the modulated symbols of the authentication message. Note that, as the last step of encoding a 2D barcode, a finder pattern should be

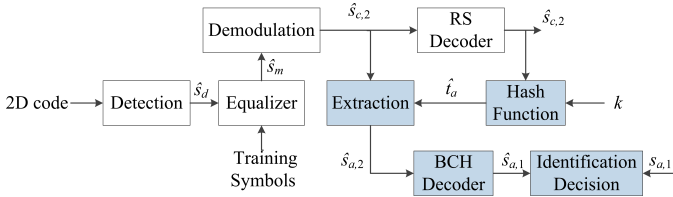


Fig. 6. Block diagram of the receiver in the proposed LCAC code.

attached to facilitate the detection of a 2D barcode reader [25]; however, without causing any confusion, the finder pattern is omitted in Fig. 2 for conciseness.

After the embed block, we obtain a signal with embedding message $s_{e,2}$. Then, through a pulse amplitude modulation (PAM) with order M [23] to yield a modulated signal s_m . After inserting the header and training symbols into the modulated signal s_m , the original version of a 2D barcode, s_d , is generated.

B. Description for the Receiver

When a printed 2D barcode is captured by a receiver, a series of standard operations should be proceeded to extract the source message. The block diagram of the receiver in the proposed LCAC Code is illustrated in Fig. 6. Similar to Fig. 1, the blue blocks represent the additional one for anti-copying but the remaining blocks are the same as those of considered 2D barcodes. The first block of a receiver is the detection block which scans the printed 2D barcode with a mobile phone camera or even optical scanner. Fig. 4(d) and Fig. 4(e) illustrate the results of the detection block in a legal 2D barcode and an illegally copied 2D barcode, respectively. Then, the detection block quantizes the mean intensity within each partitioned area to obtain a gray-scale signal \hat{s}_d .

In the verification process, the receiver first generates the estimated embedding locations \hat{t}_a using (3) with the secret key k . And, the \hat{t}_a can be generated without error ($\hat{t}_a = t_a$) even when $\hat{s}_{c,1}$ contains some error since $g(\cdot)$ is robust against input error, e.g., robust hash functions [29], [30]. According to the location specified by \hat{t}_a , the receiver extracts $\hat{s}_{a,2}$ from $\hat{s}_{c,2}$ through the extraction block and decodes it via a BCH Decoder to obtain $\hat{s}_{a,1}$. By comparing the values of $\hat{s}_{a,1}$ and $s_{a,1}$, the receiver makes a final authentication decision. For example, if the number of different bits between $\hat{s}_{a,1}$ and $s_{a,1}$ is beyond a predetermined threshold δ , the questioned 2D barcode is judged as an illegal one; otherwise, it is a legal one. The specific value of threshold δ is determined by exploiting the characteristics of the illegal channel. The model analysis of illegal channel and parameter optimization of the proposed LCAC code are presented in the following two sections, Section IV, Section V, respectively.

IV. THEORETICAL MODELING OF AN ILLEGAL CHANNEL

This section describes the modeling process of an illegal channel based on various printers and scanners. A typical Print & Scan channel introduces several types of distortions, e.g., intensity variation, scaling, rotation, low-pass filtering,

TABLE I
DESCRIPTION OF PRINTERS, SCANNERS AND A MOBILE PHONE

Name	Model	Resolution
Laser Printer 1 (P_1)	HP LaserJet P1108	1200 DPI
Laser Printer 2 (P_2)	FUJI P355D	600 DPI
CCD Scanner 1 (S_1)	BENQ K810	1200 DPI
CCD Scanner 2 (S_2)	EPSON V330	600 DPI
Mobile Phone (M)	HONOR V20	48 MP

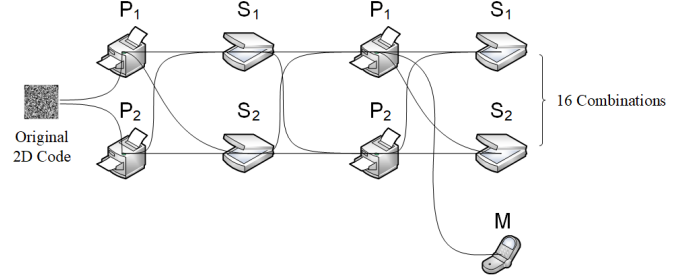


Fig. 7. Combinations of 2 printers, 2 scanners and 1 mobile phone to emulate a DPS process.

aliasing, and noise. The single print & scan (SPS) process has been modeled and analyzed [12]. In this work, a series of experiments have been conducted to model an illegal channel in a DPS process. The devices used and the corresponding parameters are listed in Tab. I, where two printers, two scanners, and one mobile phone are chosen from various manufacturers. Here, the remaining parameters of these devices are set as their default values.

Without loss of generality, the source and authentication messages are uniformly generated as two random sequences, thus, the number of symbols in different constellations are roughly equal. As illustrated in Fig. 7, a total of 16 combinations is available to emulate a DPS process with 2 printers and 2 scanners in Tab. I plus one combination of $P_1-S_1-P_1-M$.

Similar to the findings in [12], by observing the experimental results, the intensity variation in the barcode over a DPS channel can be modeled with a generalized Gaussian distribution (GGD). For a GGD random variable (RV), i.e., $X \sim \mathcal{GGD}(\mu, \sigma^2, \gamma)$ there are three parameters, including the mean μ , the variance σ^2 , and the shape factor γ . According to [31], the PDF and CDF of X can respectively be given as

$$f_X(x) = \frac{\gamma \eta(\sigma, \gamma)}{2\Gamma(1/\gamma)} \exp[-(\eta(\sigma, \gamma)|x - \mu|)^\gamma], \quad (4)$$

and

$$F_X(x) = \frac{1}{2} + \text{sgn}(x - \mu) \frac{\kappa[1/\gamma, (|x - \mu| \eta(\sigma, \gamma))^\gamma]}{2\Gamma(1/\gamma)}, \quad (5)$$

where $\eta(\sigma, \gamma) = \frac{1}{\sigma} \sqrt{\frac{\Gamma(3/\gamma)}{\Gamma(1/\gamma)}}$, $\kappa(\cdot)$ is the lower incomplete gamma function, $\Gamma(\cdot)$ is the gamma function, and $\text{sgn}(x)$ represents a symbol decision function, i.e., $\text{sgn}(x) = 1$, if $x \geq 0$, and $\text{sgn}(x) = -1$ otherwise.

Now we introduce how to estimate three parameters of a GGD distribution from experimental results. For a PAM signal with order M , the transmitted signal is denoted by x_i , ($i = 1, 2, \dots, M$), and the corresponding received signal through a channel is denoted by $y_j(j)$, ($j = 1, 2, \dots, J$), where J is the total number of experimental results on each

constellation point. Following [32], the sample mean μ_i and sample variance σ_i^2 of $y_i(j)$ are obtained as

$$\mu_i = \frac{1}{J} \sum_{j=1}^J y_i(j), \quad (6)$$

$$\sigma_i^2 = \frac{1}{J-1} \sum_{j=1}^J [y_i(j) - \mu_i]^2. \quad (7)$$

The estimation of the shape factor γ_i is more difficult than the other two parameters. According to the results of [33], [34], we obtain generalized Gaussian ratio function $r(\gamma_i)$ which is a function of γ_i and is defined as

$$r(\gamma_i) = \frac{\sigma_i^2}{\left(\frac{1}{J} \sum_{j=1}^J |y_i(j) - \mu_i(j)|\right)^2} = \frac{\Gamma(1/\gamma_i)\Gamma(3/\gamma_i)}{\Gamma^2(2/\gamma_i)}. \quad (8)$$

By setting $r(\gamma_i) = \rho_i$, a feasible solution of γ_i can be found as

$$\gamma_i = r^{-1}(\rho_i), \quad (9)$$

where an exhausted search approach is employed for solving the (9) to obtain an estimate of γ_i . Then, the value of γ_i gradually increases from zero and the search process is completed until $r(\gamma_i) = \rho_i$. Although the GGD has been also employed in [12] to model the channel of a 2D barcode, there is a fundamental difference. It only considers the model of an SPS process rather than a DPS process in an illegal copying attack.

V. EXPERIMENT RESULTS

A. Experimental Results of Channel Modeling

In our experiment, the parameters of our approach are given as follows: $k = 440$ bits, $n = 2040$ bits, $t = 800$, $k_a = 147$ bits, $n_a = 255$ bits, $t_a = 14$, $N = 2$, $L_s = 4080$ bits, $L_h = 338$ bits, and $L_t = 4418$ bits. Unless otherwise specified, our experiments follow these settings. First, the printing material is chosen as the A4 paper with weight 120g/m^2 from the Xerox. Second, an original 2D barcode with $L_t = 47 \times 47$ modules is printed on the chosen paper, where the printed size of each barcode is set as $3.2 \times 3.2 \text{ cm}^2$. Last but not least, each combination is repeated 72 times to obtain the average results. The general experimental settings are summarized as follows:

- Printing 1: HP LaserJet P1108 printer in 1200 DPI on paper with 120 grams per square meter (gsm), and a rendering size of $3.2 \times 3.2 \text{ cm}^2$;
- Printing 2: FUJI P355D printer in 600 DPI on paper with 120 gsm, and a rendering size of $3.2 \times 3.2 \text{ cm}^2$;
- Scanning 1: BENQ K810 scanner in 1200 DPI;
- Scanning 2: EPSON V330 scanner in 600 DPI;
- Camera Phone: HONOR V20 with 48 MP resolution;
- Barcode Design: A multilevel barcode with 47×47 modules;
- Capture Angle: Within 10 degrees between the barcode image plane and the camera sensor plane;
- Capture Distance: About 15 cm in the in-focus case.

- Lighting: 300–350 lux for the bright case and 100–150 lux for the dim case.

Four metrics of bit error rates (BERs) can be calculated to characterize the reception performance against channel distortion. The first two metrics are used to measure the robustness of the authentication message. The first metric is the demodulated BER of the authentication message $\varepsilon_{a,2}$ which is calculated by comparing $\hat{s}_{a,2}$ and $s_{a,2}$, while the second metric is the decoded BER of the authentication message, $\varepsilon_{a,1}$, obtained by comparing $\hat{s}_{a,1}$ and $s_{a,1}$. Moreover, the remaining two metrics are used to represent the robustness of the source message, which also represents the covertness of the proposed LCAC code. The third metric is the demodulated BER of the source message, $\varepsilon_{c,2}$ computed by comparing $\hat{s}_{c,2}$ and $s_{c,2}$, while the fourth metric is the decoded BER of the source message, $\varepsilon_{c,1}$ by comparing $\hat{s}_{c,1}$ and $s_{c,1}$, and determined by the following formula: $\varepsilon_{c,1} = |\hat{\varepsilon}_{c,1} - \varepsilon_{c,1}|_0 / NK$.

According to (6), (7) and (9), the estimation results of three parameters of illegally copied 2D barcode under 16 combinations are given in Tab. II. We accumulated the 72 samples obtained from each combination, and the blocks corresponding to the four gray values were superimposed respectively to calculate the frequency of the actual gray values. Then the corresponding histogram of the received signal constellations in an illegally copied 2D barcode and GGD approximation are shown in Fig. 8. We can see that the experimental results match well with a GGD approximation for all constellations except $x_1 = 40$. It is conjectured that since the points of $x_1 = 40$ have the lowest intensity level as compared with the other constellations, which is more sensitive to the distortions in an illegal copying process [24].

Moreover, from Fig. 8, we can also obtain the following observations. First, by comparing the results of the subfigures in the first two rows of Fig. 8 with those in the last two rows, we find that the sample mean of $x_4 = 220$ in the former group is larger than those in the latter group, which is due to the different printers in the first printing process. Second, by comparing the results of the subfigures in the first and the third rows of Fig. 8 with those in the second and fourth rows, we find that the peak value of histogram at $x_1 = 40$ in the former group is smaller than those in the latter group, *i.e.*, about 0.05 and 0.15, which is determined by the chosen scanner in the first scanning process; Finally, by comparing the results of the subfigures in the first and third columns of Fig. 8 with those in the second and fourth columns, we find that the peak value of histogram at $x_1 = 40$ in the former group is smaller than those in the latter group, which is determined by the chosen scanner in the second scanning process.

B. Advanced Illegal Copying Strategy

The experimental results given in the previous subsection are based on a simple illegal copying strategy, *i.e.*, direct-copying (DC) attack. If an attacker can capture multiple printed samples of the same legal 2D barcode, he or she can utilize all samples to improve the probability of a successful attack. For example, the attacker first generates a synthesized 2D barcode with better quality by averaging the intensities

TABLE II
ESTIMATED PARAMETERS OF A GGD APPROXIMATION FOR ILLEGALLY COPIED 2D BARCODES UNDER 16 COMBINATIONS.

(a) $P_1 - S_1 - P_1 - S_1$				(b) $P_1 - S_1 - P_1 - S_2$				(c) $P_1 - S_1 - P_2 - S_1$				(d) $P_1 - S_1 - P_2 - S_2$			
x	$\mu(x)$	$\sigma^2(x)$	$\gamma(x)$	x	$\mu(x)$	$\sigma^2(x)$	$\gamma(x)$	x	$\mu(x)$	$\sigma^2(x)$	$\gamma(x)$	x	$\mu(x)$	$\sigma^2(x)$	$\gamma(x)$
40	38.63	138.53	1.34	40	33.71	115.09	1.28	40	30.99	156.18	1.22	40	31.02	124.53	1.15
100	119.87	432.05	1.77	100	106.77	405.33	1.73	100	110.31	351.84	1.75	100	107.25	276.83	1.67
160	169.03	333.62	1.93	160	175.59	242.49	1.96	160	171.46	217.05	1.98	160	168.13	252.68	1.94
220	215.83	120.37	1.76	220	211.03	128.23	1.91	220	210.87	112.96	1.99	220	218.78	216.23	1.96
(e) $P_1 - S_2 - P_1 - S_1$				(f) $P_1 - S_2 - P_1 - S_2$				(g) $P_1 - S_2 - P_2 - S_1$				(h) $P_1 - S_2 - P_2 - S_2$			
x	$\mu(x)$	$\sigma^2(x)$	$\gamma(x)$	x	$\mu(x)$	$\sigma^2(x)$	$\gamma(x)$	x	$\mu(x)$	$\sigma^2(x)$	$\gamma(x)$	x	$\mu(x)$	$\sigma^2(x)$	$\gamma(x)$
40	24.83	34.01	0.84	40	23.38	24.83	0.65	40	31.48	29.65	0.94	40	30.55	23.02	0.87
100	100.54	385.77	1.83	100	97.87	348.76	1.73	100	105.64	429.72	2.35	100	100.79	401.96	2.26
160	160.95	267.73	1.95	160	159.89	273.04	1.91	160	161.22	221.04	2.11	160	159.54	272.79	2.05
220	202.44	132.34	1.81	220	207.91	190.38	1.91	220	203.75	103.07	1.72	220	214.87	194.64	1.71
(i) $P_2 - S_1 - P_1 - S_1$				(j) $P_2 - S_1 - P_1 - S_2$				(k) $P_2 - S_1 - P_2 - S_1$				(l) $P_2 - S_1 - P_2 - S_2$			
x	$\mu(x)$	$\sigma^2(x)$	$\gamma(x)$	x	$\mu(x)$	$\sigma^2(x)$	$\gamma(x)$	x	$\mu(x)$	$\sigma^2(x)$	$\gamma(x)$	x	$\mu(x)$	$\sigma^2(x)$	$\gamma(x)$
40	24.91	85.63	1.22	40	26.33	72.71	1.16	40	29.21	110.79	1.38	40	33.69	79.32	1.44
100	114.92	323.97	2.16	100	114.82	246.74	2.09	100	111.27	238.01	2.07	100	103.29	198.15	2.01
160	165.03	226.41	1.98	160	164.29	198.53	1.93	160	166.02	158.36	1.99	160	165.97	294.82	1.84
220	198.55	124.51	1.99	220	201.43	128.01	2.01	220	188.91	76.36	1.86	220	202.22	220.46	1.88
(m) $P_2 - S_2 - P_1 - S_1$				(n) $P_2 - S_2 - P_1 - S_2$				(o) $P_2 - S_2 - P_2 - S_1$				(p) $P_2 - S_2 - P_2 - S_2$			
x	$\mu(x)$	$\sigma^2(x)$	$\gamma(x)$	x	$\mu(x)$	$\sigma^2(x)$	$\gamma(x)$	x	$\mu(x)$	$\sigma^2(x)$	$\gamma(x)$	x	$\mu(x)$	$\sigma^2(x)$	$\gamma(x)$
40	25.41	31.56	0.96	40	25.14	24.09	0.82	40	30.64	21.97	0.85	40	22.11	22.59	0.64
100	111.59	217.18	1.88	100	105.02	177.93	1.82	100	103.56	215.04	2.24	100	108.63	260.99	2.18
160	160.26	172.17	1.92	160	156.64	212.76	1.89	160	152.81	183.35	2.03	160	163.53	208.76	1.99
220	198.09	124.09	2.02	220	209.84	276.31	1.91	220	187.54	139.71	2.17	220	196.91	139.13	2.19

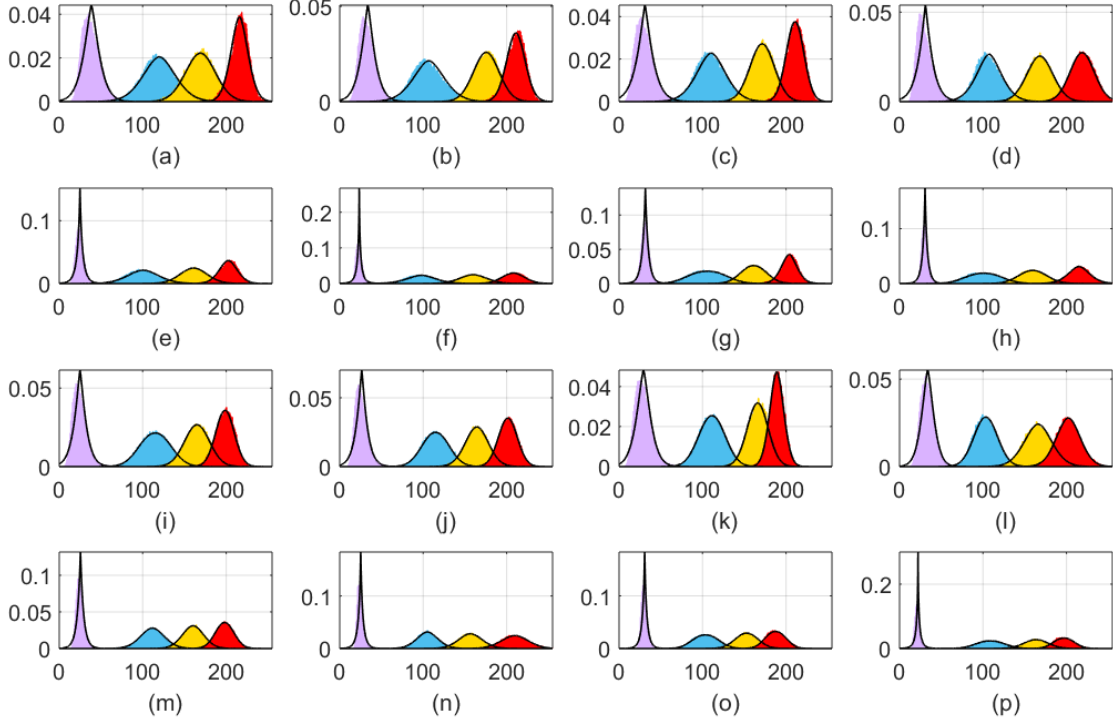


Fig. 8. Histograms of the received intensities in an illegally copied 2D barcode and the approximation curves of GGD models under 16 combinations: (a) $P_1 - S_1 - P_1 - S_1$; (b) $P_1 - S_1 - P_1 - S_2$; (c) $P_1 - S_1 - P_2 - S_1$; (d) $P_1 - S_1 - P_2 - S_2$; (e) $P_1 - S_2 - P_1 - S_1$; (f) $P_1 - S_2 - P_1 - S_2$; (g) $P_1 - S_2 - P_2 - S_1$; (h) $P_1 - S_2 - P_2 - S_2$; (i) $P_2 - S_1 - P_1 - S_1$; (j) $P_2 - S_1 - P_1 - S_2$; (k) $P_2 - S_1 - P_2 - S_1$; (l) $P_2 - S_1 - P_2 - S_2$; (m) $P_2 - S_2 - P_1 - S_1$; (n) $P_2 - S_2 - P_1 - S_2$; (o) $P_2 - S_2 - P_2 - S_1$; (p) $P_2 - S_2 - P_2 - S_2$.

over all received barcode samples and then illegally prints it. This strategy is termed as a synthesized-copying (SC) attack.

For convenience, the device combination of $P_1 - S_1 - P_1 - S_1$

is chosen to emulate an SC attack. We still use a GGD to model an SC attack, i.e., $(GGD(\mu_i(n_s), \sigma_i^2(n_s), \gamma_i(n_s)))$, where n_s is the number of synthesized samples. Similar to the

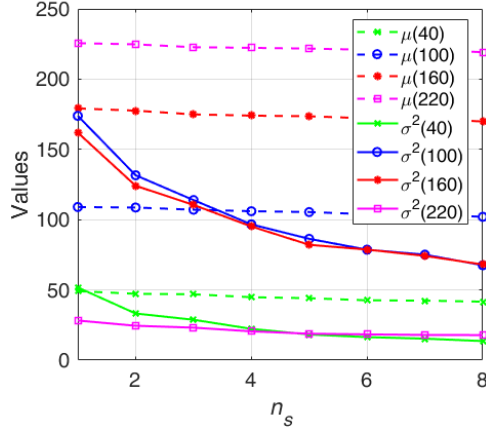


Fig. 9. Estimated parameters of an SC attack for an attacker's receiver.

equations from (6) to (9), three parameters are obtained as

$$\mu_i(n_s) = \frac{1}{J} \sum_{j=1}^J \left(\frac{1}{n_s} \sum_{s=1}^{n_s} y_i(s, j) \right), \quad (10)$$

$$\sigma_i^2(n_s) = \frac{1}{J-1} \sum_{j=1}^J \left(\left(\frac{1}{n_s} \sum_{s=1}^{n_s} y_i(s, j) \right) - \mu_i(n_s) \right)^2, \quad (11)$$

$$\gamma_i(n_s) = r^{-1}(\rho_i(n_s)), \quad (12)$$

where

$$\rho_i(n_s) = \frac{\sigma_i^2(n_s)}{\left(\frac{1}{J-1} \sum_{j=1}^J \left| \left(\frac{1}{n_s} \sum_{s=1}^{n_s} y_i(s, j) \right) - \mu_i(n_s) \right| \right)^2}. \quad (13)$$

Note that if $n_s = 1$, an SC attack reduces to a DC attack.

1) *Experimental Results at an Attack's Receiver:* The estimated parameters of an SC attack with (10), (11) and (12) are presented in Fig. 9. We can see that as n_s increases, the sample mean gradually closes the corresponding ideal constellation point, and the sample variance decreases as expected. However, the decrease rates of the variance become slower gradually. For example, by comparing the case of $n_s = 1$ for $x_4 = 220$ with that of $n_s = 2$, the variance is decreased from 28.20 to 24.48 and the decreasing ratio is $(28.20 - 24.48) / 28.20 = 13.19\%$. In contrast, by comparing the case of $n_s = 7$ for $x_4 = 220$ with that of $n_s = 8$, the variance is only decreased from 17.94 to 17.84 and the decreasing ratio is $(17.94 - 17.84) / 17.94 = 0.56\%$. Thus, we can draw an important conclusion of an SC attack: although a synthesized operation can improve attack accuracy, this improvement gradually approaches a bottleneck.

2) *Experimental Results at a Legal Receiver:* Through a synthesized operation, an attacker generates 2D barcode and prints it on a paper. Then, the legal receiver can scan it and perform authentication to detect an illegal copying 2D barcode. Now, we present the BERs analysis of an SC attack for a legal receiver, where both scanner and mobile phone are considered as the capturing device of a legal receiver, as shown in Fig. 10 and Fig. 11, respectively. From Fig. 10 and

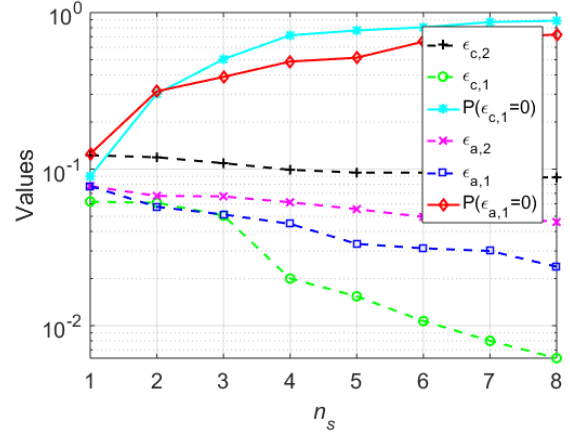


Fig. 10. BERs analysis of an SC attack for a legal receiver (Scanner).

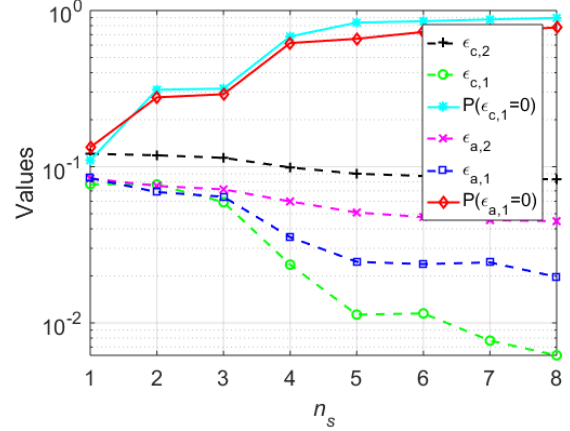


Fig. 11. BERs analysis of an SC attack for a legal receiver (Mobile Phone).

Fig. 11, we can see that as n_s increases, the values of all BERs are decreased as expected. At the same time, the probability that the BERs is equal to 0 also increases gradually with the increase of n_s . For example, as shown in Fig. 10, when $n_s = 1$, $\mathbb{P}(\epsilon_{c,1} = 0) = 0.0909$ and $\mathbb{P}(\epsilon_{a,1} = 0) = 0.1250$; when $n_s = 8$, $\mathbb{P}(\epsilon_{c,1} = 0) = 0.8871$ and $\mathbb{P}(\epsilon_{a,1} = 0) = 0.7258$. Here, $\mathbb{P}(\cdot)$ denotes a probability measure. Moreover, by compare the results of Fig. 11 with those of Fig. 10, we find that the results under a mobile phone is better than those under a scanner. For example, as shown in Fig. 11, when $n_s = 1$, $\mathbb{P}(\epsilon_{c,1} = 0) = 0.1102$ and $\mathbb{P}(\epsilon_{a,1} = 0) = 0.1338$; when $n_s = 8$, $\mathbb{P}(\epsilon_{c,1} = 0) = 0.8978$ and $\mathbb{P}(\epsilon_{a,1} = 0) = 0.7790$. The advantage under a mobile phone is because the selected mobile phone has better capturing resolution than that under the selected scanner, which is further verified in the next section by comparing the bias from the standard constellation point to the recovered constellation point. Note that, since the channel distortions in a DPS process are more severe than those of an SPS process, the legal receiver cannot always decode both the source and authentication messages without errors.

3) *Verification Decision in the Proposed LCAC code:* Note that the main objective of this paper is to find an effective

and low-cost approach to authenticate an illegal copying 2D barcode. Based on the experimental results of both Fig. 10 and Fig. 11, we consider two authentication approaches. In the first approach, the authentication decision is made by checking whether the source message can be ideally decoded, *i.e.*, $\varepsilon_{c,1} = 0$. In the second approach, the authentication decision is made by checking whether the authentication message can be ideally decoded, *i.e.*, $\varepsilon_{a,1} = 0$. Thus, the results of both $\mathbb{P}(\varepsilon_{c,1} = 0)$ and $\mathbb{P}(\varepsilon_{a,1} = 0)$ are also provided in both Fig. 10 and Fig. 11.

Although the first authentication approach is simple even no embedding of authentication message, it has two obvious drawbacks. First, as n_s increases, the value of $\mathbb{P}(\varepsilon_{c,1} = 0)$ is obviously increased, which lowers the efficiency of the first approach. Second, the parameters of a source message are predetermined according to certain considered of a 2D barcode, and it cannot be arbitrarily changed for improving the authentication accuracy. In contrary, the second authentication approach is a better option, although the value of $\mathbb{P}(\varepsilon_{a,1} = 0)$ is also increased as n_s increases. This is because the parameters of an authentication message are freely adjustable to improve the authentication accuracy, which overcomes the second drawback of the first authentication approach and is the most attractive feature of the proposed LCAC code. Therefore, we use the second authentication approach as the authentication decision block of the receiver in the proposed LCAC code, as shown in Fig. 6, which is specifically described as the following definition.

Definition 1: The authentication decision block of the receiver in the proposed LCAC code identifies the captured 2D barcode as an illegal copying one, if $\varepsilon_{a,1} > \delta$, where $0 \leq \delta < 1$ is a threshold of the authentication decision.

Note that a smaller value of δ corresponds to higher security, *e.g.*, $\delta = 0$ indicates that the captured 2D barcode is identified as an illegal copying one if there is any decoded error. However, a false rejection decision may accidentally occur, since there is also a decoded error ($\varepsilon_{a,1} \neq 0$) for a legal 2D barcode under some unideal situations, *e.g.*, the resolution of a capturing device is not sufficiently high or the lighting is poor. Thus, the value of δ should not be set too small to avoid false decision. On the contrary, the value of δ also should not be set too large, otherwise, it will increase the success possibility of illegally-copying attacks. In the next section, the criterion for selecting δ will be discussed based on the chosen device and the parameters of the proposed LCAC code can then be optimized.

VI. OPTIMIZATION OF EMBEDDING PARAMETERS

In this section, we optimize the parameters of the proposed LCAC 2D barcode in order to increase the cost of copying attack and achieve a better anti-copying effect, which consists of four steps. First, the experimental results of modeling for an SC attack is presented. Second, based on the modeling results, a prediction function is established. Third, based on the prediction function, the parameters of the proposed LCAC code will be optimized. Finally, the selection of δ is discussed and experimental results are given.

A. Experimental Results of Modeling for an SC Attack

Although the modeling results of an SC attack given in the previous subsection work well, it is mathematically intractable to obtain an exact theoretical expression for the sum of multiple GGD RVs. Thus, we propose a simple method to simplify the process of establishing the prediction function. First, following [35], we assume the sum of multiple GGD RVs can be approximated by a new GGD RV, *i.e.*, $\mathcal{GGD}(\hat{\mu}_f, \hat{\sigma}_f^2, \hat{\gamma}_f)$. Then the three parameters of the new GGD RV can be estimated as follows. It should be noted that we have fitted all three parameters of the curve, which is a process of correction. According to the actual fluctuations of each parameter, we used a variety of common curve fitting functions (Exponential, Gaussian, Linear Fitting, Polynomial, Power with one term or two terms and so on) for correction, and finally chose one of them with the smallest error.

According to (10), (11) and (12), the estimates of three parameters of a GGD approximation for an SC attack under 8 cases under a mobile phone are given in Tab. III. Then the corresponding normalized histogram of the received signal points in an illegally copied 2D barcode and GGD approximation for an SC attack are given in Fig. 12. Similar to Fig. 8, Fig. 12 shows that the experimental results match well with a GGD approximation for all constellation points except $x_1 = 40$. As n_s increases, we obtain two conclusions. First, the sample mean of all received signal points gradually close the ideal constellation point. Second, the sample variance of all received signal points gradually decreases except that $x_4 = 220$, which indicates the complexity of a DPS process and the model is more accurate in the mid-range region of the histogram.

B. Prediction Function

In the previous section, through experimental results, we find that as n_s increases, the success possibility of an SC attack is increased. It is desirable to optimize the parameters of the proposed LCAC code (k_a , n_a and δ) to lower the success possibility of an SC attack. In other words, the attacker has to increase the value of n_s to satisfy the condition of authentication decision, *i.e.*, $\varepsilon_{a,1} > \delta$. The attacker is required to obtain more numbers of legal 2D barcodes from the manufacturer, which significantly increases the cost of illegally-copying attacks. If the manufacturer can predict the value of n_s , the used times of a 2D barcode can be determined to make a tradeoff between the costs of production and illegal copying. Specifically, a larger n_s corresponds to a lower production cost but increase the cost of illegally-copying attacks and vice versa. An extreme case is that if the 2D barcode generated by the merchant is unique, then his production cost is very high, and the return is that the attacker cannot generate an illegal 2D barcode through synthetic attacks. So we need to make a trade-off to estimate a reasonable n_s .

It is tedious and difficult to predict the value of n_s by modeling an SC attack based on various experiments and all numbers of synthesized samples. It is even impossible under certain situation, *e.g.*, the device used by an attacker is unknown to the manufacturer. Thus, this paper considers a feasible solution to predict the value of n_s . Specifically, we first

TABLE III
ESTIMATED PARAMETERS OF A GGD APPROXIMATION FOR AN SC ATTACK UNDER 8 CASES (MOBILE PHONE).

(a) $n_s = 1$				(b) $n_s = 2$				(c) $n_s = 3$				(d) $n_s = 4$			
x	$\mu(x)$	$\sigma^2(x)$	$\gamma(x)$	x	$\mu(x)$	$\sigma^2(x)$	$\gamma(x)$	x	$\mu(x)$	$\sigma^2(x)$	$\gamma(x)$	x	$\mu(x)$	$\sigma^2(x)$	$\gamma(x)$
40	41.06	119.24	1.39	40	40.45	94.92	1.39	40	40.66	92.70	1.33	40	38.77	78.34	1.33
100	117.61	474.53	1.91	100	116.55	470.69	1.72	100	116.17	431.69	1.79	100	112.63	418.92	1.87
160	167.05	378.64	2.18	160	171.53	348.23	2.04	160	165.71	345.62	1.98	160	163.50	325.93	1.78
220	214.92	129.37	1.76	220	218.60	113.73	1.79	220	212.48	126.68	1.81	220	212.21	121.21	1.72
(e) $n_s = 5$				(f) $n_s = 6$				(g) $n_s = 7$				(h) $n_s = 8$			
x	$\mu(x)$	$\sigma^2(x)$	$\gamma(x)$	x	$\mu(x)$	$\sigma^2(x)$	$\gamma(x)$	x	$\mu(x)$	$\sigma^2(x)$	$\gamma(x)$	x	$\mu(x)$	$\sigma^2(x)$	$\gamma(x)$
40	39.76	71.82	1.44	40	39.94	73.17	1.41	40	39.14	79.49	1.42	40	38.25	71.40	1.26
100	111.42	414.32	1.65	100	111.09	412.73	1.66	100	111.14	400.48	1.64	100	110.30	393.58	1.61
160	163.70	315.48	1.92	160	163.81	307.67	1.94	160	164.69	292.47	1.95	160	164.88	282.19	1.83
220	212.41	106.46	1.81	220	212.76	97.87	1.71	220	214.03	93.28	1.72	220	213.33	87.11	1.63

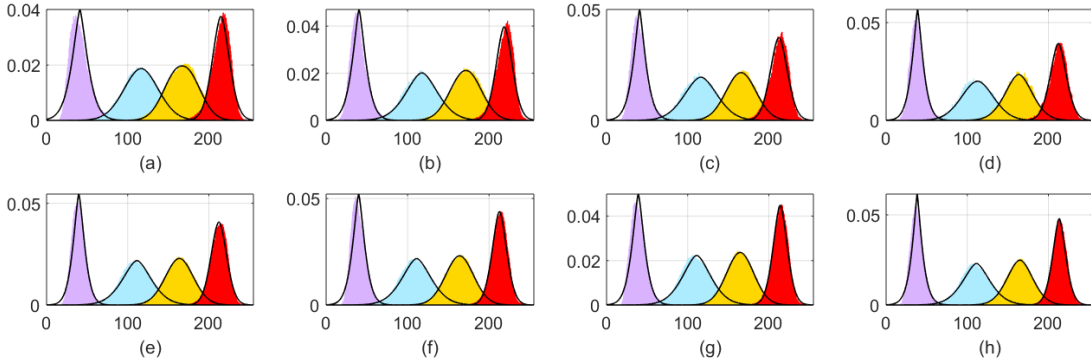


Fig. 12. Histograms of the received intensities in an illegally copied 2D barcode and the approximation curves of GGD models for an SC attack under 8 cases: (a) $n_s = 1$; (b) $n_s = 2$; (c) $n_s = 3$; (d) $n_s = 4$; (e) $n_s = 5$; (f) $n_s = 6$; (g) $n_s = 7$; (h) $n_s = 8$ (Mobile Phone).

establish a prediction function based on the modeling results of an SC attack with a finite number of synthesized samples. Then, based on the prediction function, the manufacturer can effectively estimate the value of n_s .

First, we use a power fitting function with two variables to estimate $\hat{\mu}_f$ as

$$\hat{\mu}_f = a_\mu f^{b_\mu}, \quad (14)$$

where f represents the estimated number of synthesized samples, two variables (a_μ and b_μ) are obtained according to $\mu_i (n_s) = a_\mu n_s^{b_\mu}$.

Second, we use a power fitting function with three variables to estimate $\hat{\sigma}_f^2$ as

$$\hat{\sigma}_f^2 = a_\sigma f^{b_\sigma} + c_\sigma, \quad (15)$$

where three variables (a_σ , b_σ , and c_σ) are obtained according to $\sigma_i^2 (n_s) = a_\sigma n_s^{b_\sigma} + c_\sigma$.

Third, since from Tab. III., we can see that the value of the shape factor fluctuates around a certain constant, we directly use an average fitting function to estimate $\hat{\gamma}_f$ as

$$\hat{\gamma}_f = \frac{1}{n_s} \sum_{s=1}^{n_s} \gamma(s). \quad (16)$$

Based on the results of Tab. III, prediction functions under a mobile phone are devised. For the mobile phone M, the estimated parameters and predicted parameters for $x_2 = 100$ are illustrated in Fig. 13, where $a_\mu = 118.6$, $b_\mu = -0.0342$, $a_\sigma = -138.5$, $b_\sigma = 0.232$, and $c_\sigma = 617.7$. From Fig. 13, we can see that the estimated parameters oscillate around

the predicted parameters, which verifies the efficacy of the prediction function.

C. Parameter Optimization

Based on a prediction function $\text{GGD}(\hat{\mu}_f, \hat{\sigma}_f^2, \hat{\gamma}_f)$, we can predict $\hat{\varepsilon}_{a,2}$ and even $\hat{\varepsilon}_{a,1}$. Due to the space limitation, we briefly introduce how to obtain $\hat{\varepsilon}_{a,2}$. First, the BER of certain constellation point x_i can be calculated as

$$\hat{\varepsilon}_i = \sum_{j=0, j+1 \neq i}^{M-1} \alpha_j \left(F_i(\theta_{j+1}) - F_i(\theta_j) \right), \quad (17)$$

where θ_j represents decision threshold, e.g., the case of $M = 4$, $\theta_0 = 0$, $\theta_1 = 70$, $\theta_2 = 130$, $\theta_3 = 190$, and $\theta_4 = 255$, α_j is a correction factor, e.g., the case of $M = 4$, $\alpha_j = \frac{1}{2}$ for $|j+1-i| \leq 2$; otherwise $\alpha_j = 1$, $F_i(\theta)$ represents a CDF based on the predicted parameters, expressed as

$$F_X(x_i) = \frac{1}{2} + \text{sgn}(x_i - \hat{\mu}_f) \frac{\kappa [1/\hat{\gamma}_f, (|x_i - \hat{\mu}_f| \eta(\hat{\sigma}_f, \hat{\gamma}_f)) \hat{\gamma}_f]}{2\Gamma(1/\hat{\gamma}_f)}. \quad (18)$$

Then the theoretical expressions of $\hat{\varepsilon}_{a,2}$ is given as

$$\hat{\varepsilon}_{a,2} = \frac{1}{M} \sum_{i=1}^M \hat{\varepsilon}_i. \quad (19)$$

Now we introduce a simple strategy of parameter optimization (δ , κ_a and n_a) for the proposed LCAC code to increase the cost of illegally-copying attacks. First, by considering the impact of embedding operation on the source message, the value of

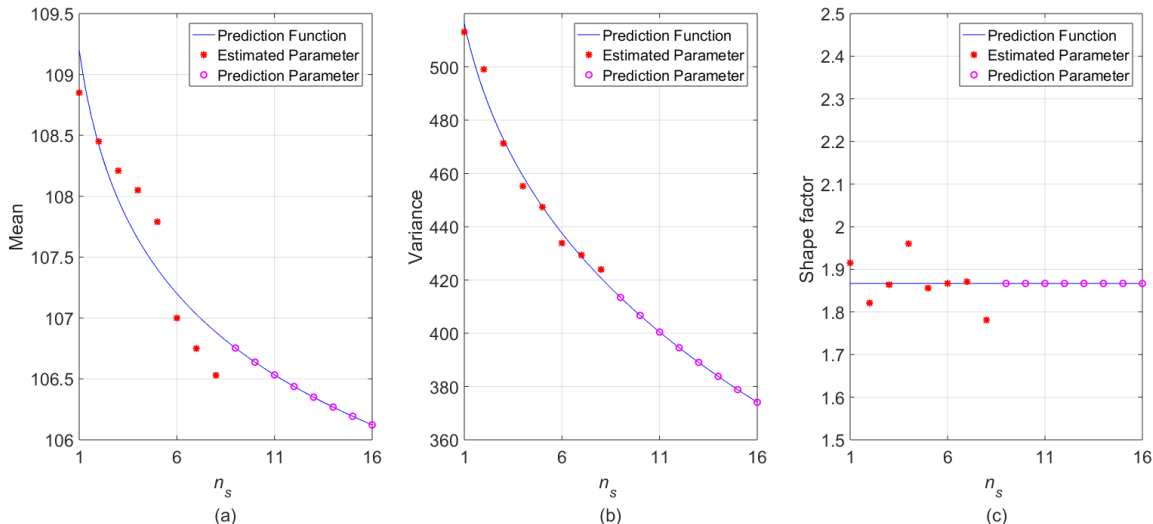


Fig. 13. Comparisons between the three estimated parameters and predicted parameters for $x_2 = 100$: (a) mean; (b) variance; (c) shape factor (Mobile Phone).

n_a is determined to satisfy the covertness requirement of the proposed LCAC code. Second, through some experimental results under a practical condition, the value of δ is determined to correctly decode the authentication message for satisfying the robustness requirement of the proposed LCAC code. At last, based on a prediction function, the value of k_a is optimized to achieve a tradeoff between the production cost and the cost of illegally-copying attacks. In the next subsection, the experimental results of the parameter optimization are presented.

D. Experimental Results

In this subsection, we present the experimental results under a mobile phone in both Fig. 14 and Fig. 15, where the other parameters are the same as those of Tab. I. Fig. 14 shows the instantaneous BER of authentication message for a legal 2D barcode, while Fig. 15 shows the average BER of authentication message for an SC attack. The authentication threshold δ is also illustrated in Fig. 14 for a comparison purpose. From Fig. 14, we can see that some non-zero instantaneous $\epsilon_{a,1}$ occurs occasionally although most of them are zero. Thus, under the current conditions, we set the value of δ as the maximum instantaneous $\epsilon_{a,1}$, i.e., $\delta = 0.012$ for satisfying the robustness requirement of the proposed LCAC code.

Fig. 15 shows the average simulation results of $\hat{\epsilon}_{a,1}$ and $\hat{\epsilon}_{a,2}$ based on a prediction function, and the theoretical results of $\hat{\epsilon}_{a,2}$ defined in (19). From Fig. 15, we can see that the average simulation results of $\hat{\epsilon}_{a,2}$ matches perfectly with the corresponding theoretical results. As the estimated number of synthesized samples increases, the values of both $\hat{\epsilon}_{a,1}$ and $\hat{\epsilon}_{a,2}$ gradually decrease as expected. Moreover, two cases of $\hat{\epsilon}_{a,1}$ ($k_a = 147$ and $k_a = 179$) are simultaneously illustrated in Fig. 15, which indicates that the $\hat{\epsilon}_{a,1}$ can be controlled by setting the value of k_a . Based on this trend, the value of k_a can be determined by making $\hat{\epsilon}_{a,1} > \delta$, when the estimated number of synthesized samples is beyond a certain value. A

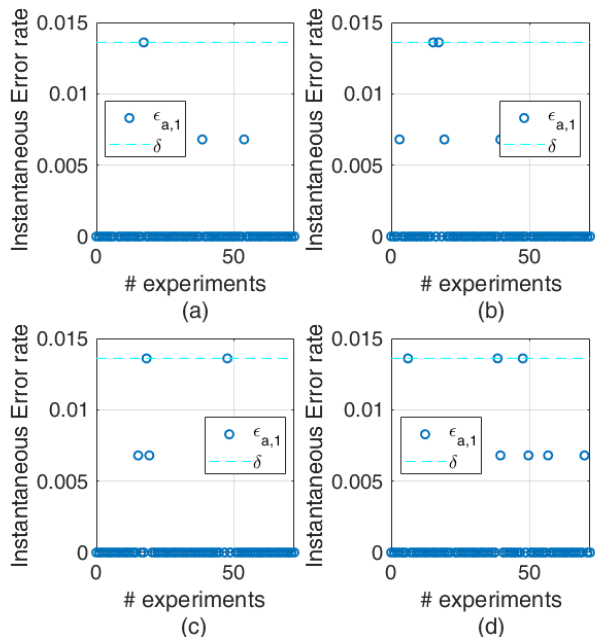


Fig. 14. Experimental results: instantaneous BER of authentication message for a legal 2D barcode in a combination of different printers and scanners, including (a) $P_1 - S_1$, (b) $P_1 - S_2$, (c) $P_2 - S_1$, and (d) $P_2 - S_2$, respectively. The x-axis represents different instances of experiments.

simple example is given as follows to verify the efficacy of the parameter optimization.

Based on the experimental conditions of Fig. 14, a BER comparison between before and after optimizations are given in Tab. IV, where the threshold is set as $\delta = 0.012$. From Tab. IV, we can see that, before optimization, the average value of $\epsilon_{a,1}$ equals to 0.0113 for an SC attack with $n_s = 10$, and even $\mathbb{P}(\epsilon_{a,1} = 0)$ equals to 84.88%. After optimization, the value of k_a is increased from 147 to 179, which indicates that the error correction capability of authentication message t_a is reduced from 14 to 10. Then, the average value of $\epsilon_{a,1}$ is increased to 0.0340 for an SC attack with $n_s = 10$, and

TABLE IV
BER COMPARISON BETWEEN BEFORE AND AFTER OPTIMIZATIONS (MOBILE PHONE)

optimization	Before			After		
Parameters	$k_a = 147, t_a = 14$ and $n_s = 10$			$k_a = 179, t_a = 10$ and $n_s = 10$		
Metrics	$\epsilon_{a,2}$	$\epsilon_{a,1}$	$\mathbb{P}(\epsilon_{a,1} = 0)$	$\epsilon_{a,2}$	$\epsilon_{a,1}$	$\mathbb{P}(\epsilon_{a,1} = 0)$
Performance	0.0342	0.0113	84.88%	0.0471	0.0340	44.71%
Parameters	N/A			$k_a = 179, t_a = 10$ and $n_s = 14$		
Metrics				$\epsilon_{a,2}$	$\epsilon_{a,1}$	$\mathbb{P}(\epsilon_{a,1} = 0)$
Performance				0.0378	0.0104	81.82%

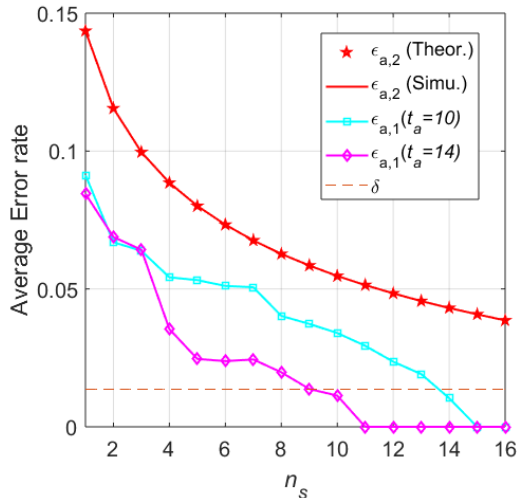


Fig. 15. Average BERs of authentication message for an SC attack under a mobile phone.

$\mathbb{P}(\epsilon_{a,1} = 0)$ obviously drops to 44.71%. While an attacker should increase the number of synthesized samples to $n_s = 14$, the probability of attack success can be improved to a similar level which happens before optimization. In other words, the results predicted in Fig. 15, $n_s = 10$ before the parameter optimization can be successfully attacked whereas $n_s = 14$ after the parameter optimization can be successfully attacked. Thus, an attacker should increase the number of synthesized samples to achieve the probability of attack success as a similar level which happens before optimization, as shown in Fig. 15. After supplementing the experiment, we can find that the prediction and optimization is still effective, that is, $n_s = 10$ before the parameter optimization, $\epsilon_{a,1} < \delta$, $n_s = 14$ after parameter optimization, $\epsilon_{a,1} < \delta$.

VII. EXTENDED EXPERIMENTAL RESULTS AND DISCUSSION

A. Comparison with Two-level QR Code

In literature, there are many existing approaches to achieve anti-copying. We choose the latest one, which is called as Two-Level QR (2LQR) code [5], to compare the performance with our approach. To the best of our knowledge, the 2LQR code is the best approach in the style of active embedding for defending against illegally-copying attacks. The basic idea of the 2LQR code is to replace all black modules of a standard QR code with some black-and-white patterns which are unknown to the third party and increases the pixel numbers of each black module. In comparison with the 2LQR code, our approach has the following advantages:

First, the 2LQR code introduces visually perceptual modification even if we do not put a 2D barcode with an embedded authentication message and a 2D barcode without that. However, our approach does not have this issue if we do not put a 2D barcode with an embedded authentication message and a 2D barcode without that at the same place. Here, we justify this conclusion by comparing the mean bias and variance of different gray values under both the 2LQR code and our approach, where the mobile phone M is considered as the capturing device. Specifically, the mean bias represents the distance from the standard constellation point to the recovered constellation point. Smaller values of the mean bias and the variance correspond to smaller visually perceptual modification. We present the experimental results in Tab. V, where we use the gray value “0” to represent the results of the 2LQR code since the 2LQR code only modifies the black part. Here, we choose two different and independent patterns to replace the black modules in the 2LQR code. Tab. V includes four cases:

- 1) Tab. V(a) represents the case that the experimental results are obtained by a mobile phone, where we do not embed the authentication message in the source message;
- 2) Tab. V(b) represents the case that the experimental results are obtained by a mobile phone, where we embed the authentication message in the source message.

Note that, in Tab. V, the bold numbers in parenthesis represent the mean bias from the standard constellation point to the recovered constellation point, which are obtained by calculating the absolute values between standard values and experimental values. From Tab. V, we can see that the 2LQR code introduces larger both mean bias and variance than our approach. By comparing the results of Tab. V(a) with those of Tab. V(b), we can see that the 2LQR code introduces significant difference for the mean and the variance due to embedding the authentication message, whereas our approach introduces a slight difference for both the mean and the variance. In summary, our approach has much better covertness performance.

Second, the 2LQR code requires higher positioning accuracy of the capturing equipment or higher proportion of the training sequence. This is because the 2LQR code requires higher resolution to capture each sub-module whereas our approach only requires the average intensity of each entire module. Third, our approach provides a theoretical model for illegal-copying 2D barcode, which is verified in Section IV. Moreover, based on the theoretical model, we optimize the parameters of our approach in order to increase the cost of copying attacks and achieve a better anti-copying effect, which

TABLE V

COMPARING THE MEAN AND VARIANCE OF OUR APPROACH WITH THOSE OF THE 2LQR CODE, WHERE WE USE “0” TO REPRESENT THE RESULTS OF THE 2LQR CODE AND THE BOLD NUMBERS IN PARENTHESIS REPRESENT THE MEAN BIAS FROM THE STANDARD CONSTELLATION POINT TO THE RECOVERED CONSTELLATION POINT.

(a) Without Embedded Authentication Message			(b) With Embedded Authentication Message		
x	$\mu(x)$	$\sigma^2(x)$	x	$\mu(x)$	$\sigma^2(x)$
0	11.45 (11.45)	21.38	0	69.42 (69.42)	225.28
40	39.89 (0.11)	17.76	40	39.64 (0.36)	23.10
100	99.57 (0.43)	154.43	100	100.75 (0.75)	151.68
160	160.06 (0.06)	129.61	160	160.29 (0.29)	143.24
220	217.77 (2.23)	31.39	220	216.61 (3.39)	39.84

TABLE VI

DECODED BER OF OUR APPROACH IN A STANDARD QR CODE.

	Mobile Phone	Scanner
$\varepsilon_{a,1}$ (SPS)	0	0
$\varepsilon_{a,1}$ (DPS)	0.0064	0.0368

is verified in Section VI. However, the 2LQR code did not provide the above features.

B. Experimental Results in Standard QR Codes

For a standard QR code, since there are only 0 and 255 gray values, it has larger tolerance level to noise as compared with the case of $M = 4$. Thus, we should reduce the error-correction capability of the authentication message. Specifically, we set $n_a = 255$ bits, $k_a = 247$ bits, and $t_a = 1$ in standard QR codes. Tab. VI provides the experimental results of our approach in a standard QR code under both Mobile Phone and Scanner. From Tab. VI, we can draw the same conclusions under the case of $M = 4$. In the SPS, all decoded BERs are zeros whereas they obviously increase in the DPS, which is also used to detect whether the received 2D barcode is illegally copied or not.

C. Discussion

By analyzing the above experimental results, we can draw the following conclusions: First, our approach does not destroy the completion of 2D barcode, since the source message in the SPS process can be successfully decoded by a legal receiver. Second, by comparing with the experimental results based on various printers, scanners, and mobile phone, it can be found that the sample histogram and curve fitting of the theoretical model match well, so it can be concluded that the theoretical model works well. Third, based on the theoretical model, we build a prediction function to optimize the parameters of our approach. The parameters optimization incorporates the covertness requirement, the robustness requirement and a tradeoff between the production cost and the cost of illegally-copying attacks together. The experimental results show that the proposed LCAC code with two printers and two scanners can detect the DC attack effectively and resist the SC attack up to the access of 14 legal copies.

VIII. CONCLUSION

In this paper, the LCAC 2D barcode was proposed, which exploited the difference between the noise characteristics of legal and illegal channels. The proposed LCAC code effectively

overcomes the drawbacks of the conventional anti-copying approaches. For accurately evaluating the performance of the proposed LCAC code, we used a GGD to model a DPS process in an illegal copying attack. By comparing with the sample histogram and curve fitting of the theoretical model, the theoretical model works well. For evaluating the security of the proposed LCAC code, besides the DC attack, the improved version which is the SC attack was also considered in this paper. We built a prediction function to optimize the parameters of the proposed LCAC code based on the theoretical model. The parameters optimization incorporated the covertness requirement, the robustness requirement and a tradeoff between the production cost and the cost of illegally-copying attacks together. The experimental results showed that the proposed LCAC code is able to prevent illegal copying effectively.

There are several promising future directions based on the proposed LCAC 2D barcode. First, it is natural to extend the gray-scale barcodes in this work to color barcodes. Although the color barcodes are more complicated than the gray-scale barcodes, both barcodes are quite similar and thus LCAC 2D color barcodes are likely able to prevent illegally copying effectively. Second, we research on detection techniques to evaluate the security level of various anti-copying 2D barcodes. At last, we use some approaches of machine learning or deep learning to improve the performance of the proposed LCAC 2D barcode.

APPENDIX A

ANALYSIS OF THE TWO EMBEDDING STRATEGIES

We consider two scenarios in practical applications of 2D barcodes: in the first scenario, there is no occlusion to emulate an ideal situation, while in the second scenario, there is a small occlusion over a 2D barcode to emulate a non-ideal situation. Three examples of a small occlusion are considered and the experimental results are given in Tab. VII. The size of occlusion is defined as $a \times b$, where a and b are the numbers of row occlusion and column occlusion, respectively. Note that the case of 0×0 represents the first scenario, in which there is no occlusion.

For the first scenario, we can see that all BERs are zeros except $\varepsilon_{c,2}$. This is because the embedding of authentication message sacrifices the robustness of the source message; however, the error-correction capabilities of encoding modules for both source and authentication messages are sufficiently powerful and channel distortion is not introduced, we obtain $\varepsilon_{c,1} = \varepsilon_{a,2} = \varepsilon_{a,1} = 0$. Moreover, we observe that $\varepsilon_{c,2}$ in Strategy 1 is smaller than that in Strategy 2, which reflects that Strategy 1 has better covertness performance than that of Strategy 2. It should be noted that this result verifies Observation 1 given in Section III.

For the second scenario, we can see that a larger occlusion size leads to higher BER values in all metrics. Moreover, two additional conclusions are drawn here. First, since the values of $\varepsilon_{c,1}$ and $\varepsilon_{c,2}$ in Strategy 1 are larger than those in Strategy 2, which is consistent with the first scenario, Strategy 1 has better performance in covertness than Strategy 2 and Observation 1

TABLE VII
ROBUSTNESS ANALYSIS OF TWO EMBEDDING STRATEGIES.

Size (in modules)	Strategy 1				Strategy 2			
	$\varepsilon_{c,2}$	$\varepsilon_{c,1}$	$\varepsilon_{a,2}$	$\varepsilon_{a,1}$	$\varepsilon_{c,2}$	$\varepsilon_{c,1}$	$\varepsilon_{a,2}$	$\varepsilon_{a,1}$
0×0	0.0313	0	0	0	0.0314	0	0	0
2×11	0.0519	0.0073	0.0230	0.0179	0.0521	0.0073	0.0211	0.0100
4×11	0.0566	0.0074	0.0256	0.0185	0.0567	0.0079	0.0247	0.0104
7×11	0.0724	0.0147	0.044	0.0339	0.0731	0.0161	0.0417	0.0224

is verified again. Second, since the values of $\varepsilon_{a,1}$ and $\varepsilon_{a,2}$ in Strategy 2 are smaller than those in Strategy 1, Strategy 2 has better robustness performance than that of Strategy 1 and Observation 2 is verified.

REFERENCES

- [1] C. Chen, B. Zhou, and W. H. Mow, "Ra code: A robust and aesthetic code for resolution-constrained applications," *IEEE Transactions on Information Forensics and Security*, vol. 11, no. 3, pp. 571–583, March 2016.
- [2] Y. Lee and W. Tsai, "A new data transfer method via signal-rich-art code images captured by mobile devices," *IEEE Transactions on Circuits and Systems for Video Technology*, vol. 25, no. 4, pp. 688–700, April 2015.
- [3] I. Tkachenko, W. Puech, O. Strauss, J. M. Gaudin, C. Destruel, and C. Guichard, "Fighting against forged documents by using textured image," in *22nd European Signal Processing Conference (EUSIPCO)*, Sep. 2014, pp. 790–794.
- [4] I. Tkachenko, W. Puech, O. Strauss, C. Destruel, and J. M. Gaudin, "Printed document authentication using two level QR code," in *2016 IEEE International Conference on Acoustics, Speech and Signal Processing (ICASSP)*, March 2016, pp. 2149–2153.
- [5] I. Tkachenko, W. Puech, C. Destruel, O. Strauss, J. Gaudin, and C. Guichard, "Two-level QR code for private message sharing and document authentication," *IEEE Transactions on Information Forensics and Security*, vol. 11, no. 3, pp. 571–583, March 2016.
- [6] C. Chen, M. Li, A. Ferreira, J. Huang, and R. Cai, "A copy-proof scheme based on the spectral and spatial barcoding channel models," to appear *IEEE Transactions on Information Forensics and Security*, pp. 1–1, 2019.
- [7] C. Wong and M. Wu, "Counterfeit detection based on unclonable feature of paper using mobile camera," *IEEE Transactions on Information Forensics and Security*, vol. 12, no. 8, pp. 1885–1899, Aug 2017.
- [8] I. Tkachenko and C. Destruel, "Exploitation of redundancy for pattern estimation of copy-sensitive two level qr code," in *2018 IEEE International Workshop on Information Forensics and Security (WIFS)*, Dec 2018, pp. 1–6.
- [9] K. Krombholz, P. Frühwirt, P. Kieseberg, I. Kapsalis, M. Huber, and E. Weippl, *QR Code Security: A Survey of Attacks and Challenges for Usable Security*. Springer International Publishing, 2014.
- [10] X. Zhu, Z. Hou, D. Hu, and J. Zhang, *Secure and Efficient Mobile Payment Using QR Code in an Environment with Dishonest Authority*. Springer International Publishing, 2016.
- [11] T. Vidas, E. Owusu, S. Wang, C. Zeng, L. F. Cranor, and N. Christin, "Qrishing: The susceptibility of smartphone users to qr code phishing attacks," *Lecture Notes in Computer Science*, vol. 7862, pp. 52–69, 2013.
- [12] R. Villán, S. Voloshynovskiy, O. J. Koval, and T. Pun, "Multilevel 2d bar codes: toward high-capacity storage modules for multimedia security and management," *IEEE Transactions on Information Forensics & Security*, vol. 1, no. 4, pp. 405–420, 2006.
- [13] X. Marguerettaz, F. Gremaud, A. Commeurec, V. Aboutanos, T. Tiller, and O. Rozumek, "Identification and authentication using liquid crystal material markings," Jun. 3 2014, uS Patent 8,740,088.
- [14] M. You, M. Lin, S. Wang, X. Wang, G. Zhang, Y. Hong, Y. Dong, G. Jin, and F. Xu, "Three-dimensional quick response code based on inkjet printing of upconversion fluorescent nanoparticles for drug anti-counterfeiting," *Nanoscale*, vol. 8, no. 19, pp. 10096–10104, 2016.
- [15] T. Maehara, K. Nakai, R. Ikeda, K. Taniguchi, and S. Ono, "Watermark design of two-dimensional barcodes on mobile phone display by evolutionary multi-objective optimization," in *International Symposium on Soft Computing and Intelligent Systems*, 2014, pp. 149–154.
- [16] S. Voloshynovskiy, T. Holtyak, and P. Bas, "Physical object authentication: Detection-theoretic comparison of natural and artificial randomness," in *IEEE International Conference on Acoustics, Speech and Signal Processing*, 2016, pp. 2029–2033.
- [17] C. W. Wong and M. Wu, "Counterfeit detection using paper pup and mobile cameras," in *IEEE International Workshop on Information Forensics and Security*, 2016, pp. 1–6.
- [18] I. Tkachenko, W. Puech, O. Strauss, J. M. Gaudin, C. Destruel, and C. Guichard, "Centrality bias measure for high density qr code module recognition," *Signal Processing Image Communication*, vol. 41, no. C, pp. 46–60, 2016.
- [19] J. Zhu, C. Du, F. Li, L. Bao, and P. Liu, "Free-electron-driven multi-frequency terahertz radiation on a super-grating structure," to appear *IEEE Access*, 2019.
- [20] Y. Zhao, Z. Fan, and M. E. Hoover, "Frequency domain infrared watermarking for printed cmyk image," in *IEEE International Conference on Image Processing*, 2011, pp. 2725–2728.
- [21] P. D. S. K. Malarchelvi, "A semi-fragile image content authentication technique based on secure hash in frequency domain," *I. J. Network Security*, vol. 15, pp. 365–372, 2013.
- [22] R. Xie, C. Hong, S. Zhu, and D. Tao, "Anti-counterfeiting digital watermarking algorithm for printed qr barcode," *Neurocomputing*, vol. 167, no. C, pp. 625–635, 2015.
- [23] M. N. Sakib and O. Liboiron-Ladouceur, "A study of error correction codes for pam signals in data center applications," *IEEE Photonics Technology Letters*, vol. 25, no. 23, pp. 2274–2277, 2013.
- [24] L. Zhang, C. Chen, and W. H. Mow, "Accurate modeling and efficient estimation of the print-capture channel with application in barcoding," *IEEE Transactions on Image Processing*, vol. 28, no. 1, pp. 464–478, 2019.
- [25] S. Rungraungsilp, M. Ketcham, V. Kosolvijak, and S. Vongpradhip, "Data hiding method for QR code based on watermark by compare DCT with DFT domain," in *3rd international conference on computer and communication technologies, India*, 2012, pp. 144–148.
- [26] A. T. P. Ho, A. M. H. Bao, W. Sawaya, and P. Bas, "Document authentication using graphical codes: reliable performance analysis and channel optimization," *Eurasip Journal on Information Security*, vol. 2014, no. 1, p. 9, 2014.
- [27] X. Wang and J. Zhao, "An improved key agreement protocol based on chaos," *Communications in Nonlinear Science and Numerical Simulation*, vol. 15, no. 12, pp. 4052 – 4057, 2010.
- [28] Y. Niu and X. Wang, "An anonymous key agreement protocol based on chaotic maps," *Communications in Nonlinear Science and Numerical Simulation*, vol. 16, no. 4, pp. 1986 – 1992, 2011.
- [29] A. Swaminathan, Y. Mao, and M. Wu, "Robust and secure image hashing," *IEEE Transactions on Information Forensics & Security*, vol. 1, no. 2, pp. 215–230, 2006.
- [30] J. Fridrich and M. Goljan, "Robust hash functions for digital watermarking," in *Information Technology: Coding and Computing, 2000. Proceedings. International Conference on*, 2000, pp. 178–183.
- [31] S. Nadarajah, "A generalized normal distribution," *Journal of Applied Statistics*, vol. 32, no. 7, pp. 685–694, 2005.
- [32] J. Franklin, "Probability theory: the logic of science," *Mathematical Intelligencer*, vol. 57, no. 10, pp. 76–77, 2004.
- [33] K. Sharifi and A. Leongarcia, "Estimation of shape parameter for generalized gaussian distributions in subband decompositions of video," *IEEE Transactions on Circuits & Systems for Video Technology*, vol. 5, no. 1, pp. 52–56, 1995.
- [34] T. Wang, H. Li, Z. Li, and Z. Wang, "A fast parameter estimation of generalized gaussian distribution," in *2006 8th international Conference on Signal Processing*, vol. 1, 2006.
- [35] H. Soury and M. S. Alouini, "New results on the sum of two generalized gaussian random variables," in *IEEE Global Conference on Signal and Information Processing*, 2015, pp. 1017–1021.